

Finite-temperature phase transition to a Kitaev spin liquid phase on a hyperoctagon lattice: A large-scale quantum Monte Carlo study

Petr A. Mishchenko, Yasuyuki Kato, and Yukitoshi Motome

Department of Applied Physics, University of Tokyo, Hongo 7-3-1, Bunkyo, Tokyo 113-8656, Japan

(Dated: February 27, 2018)

The quantum spin liquid is an enigmatic quantum state in insulating magnets, in which conventional long-range order is suppressed by strong quantum fluctuations. Recently, an unconventional phase transition was reported between the low-temperature quantum spin liquid and the high-temperature paramagnet in the Kitaev model on a three-dimensional hyperhoneycomb lattice. Here, we show that a similar “liquid-gas” transition takes place in another three-dimensional lattice, the hyperoctagon lattice. We investigate the critical phenomena by adopting the Green-function based Monte Carlo technique with the kernel polynomial method, which enables systematic analysis of up to 2048 sites. The critical temperature is lower than that in the hyperhoneycomb case, reflecting the smaller flux gap. We also discuss the transition on the basis of an effective model in the anisotropic limit.

PACS numbers: Valid PACS appear here

I. INTRODUCTION

The quantum spin liquid (QSL) is an exotic magnetic state of matter in solids, in which long-range ordering is suppressed by strong quantum fluctuations even in the ground state¹⁻³. As a consequence of intensive study over several decades, substantial progress has been recently made in experimental search for QSLs⁴⁻¹¹. In such experiments, however, QSLs are usually identified by the absence of any phase transition to a long-range ordered state. In other words, it is supposed that the low-temperature (T) QSL is adiabatically connected to the high- T paramagnetic state. This common belief relies on the magnetic analog of liquid helium 3 which remains as a liquid down to the lowest T due to strong quantum fluctuations¹. Nonetheless, in conventional fluids, gas and liquid can be distinguished by a phase transition. Hence, a similar phase transition can also be expected in the case of magnetic states of matter, namely, between the “spin gas” (paramagnet) and “spin liquid” (QSL). However, the thermodynamics of QSLs remains elusive, despite the crucial importance for understanding of existing and forthcoming experiments.

Recently, an exotic finite- T phase transition between the low- T QSL and the high- T paramagnet was reported for an extension of the Kitaev model defined on a three-dimensional (3D) hyperhoneycomb lattice as well as its anisotropic limit^{12,13}. The Kitaev model is an exactly-soluble quantum spin model, whose ground state provides a canonical example of QSLs¹⁴, and has attracted attention as it might describe the magnetism in some spin-orbit entangled Mott insulators¹⁵. The finding of the exotic phase transition was brought by a newly-developed quantum Monte Carlo (QMC) method based on a Majorana fermion representation, which is free from the negative sign problem. This phase transition is not accompanied by any symmetry breaking, but can be explained by a proliferation of loops for excited Z_2 fluxes^{12,13,16}. The emergent loop degree of freedom is specific to 3D;

the finite- T phase transition is absent and turns into a crossover in two dimensions¹⁷. The surprising result urges reconsideration of both experimental and theoretical quests for QSLs.

As demonstrated in the hyperhoneycomb case¹⁸, the Kitaev model can be extended to any tri-coordinate lattices¹⁹⁻²². Although all the extensions retain the QSL nature²³, the exact ground state (the spatial configuration of Z_2 fluxes) is obtained for some limited cases because Lieb’s theorem is not applicable to generic tri-coordinate lattices²⁴. Moreover, finite- T properties have not been studied in most cases. As there are a variety of 3D tri-coordinate lattices^{20,25}, it is interesting to investigate such 3D models for clarifying the universal aspects of the phase transition between the QSL and the paramagnet and for exploring further exotic phase transitions.

In this paper, we investigate finite- T properties in the Kitaev model on another 3D lattice, the hyperoctagon lattice²¹ (see Fig. 1). For this model, the exact solution is not available, as Lieb’s theorem cannot be applied. Improving the QMC method by employing the Green function technique with the kernel polynomial method (KPM), we compute much larger systems compared to the previous studies. From the systematic analysis of clusters up to 2048 sites, we find that the hyperoctagon model exhibits another example of finite- T phase transitions between the QSL and the paramagnet. We find that the critical temperature estimated from the careful analysis of the finite-size effects is lower than that for the hyperhoneycomb case, reflecting the smaller flux gap^{16,20}. In addition, we show that the anisotropic limit of the hyperoctagon model becomes equivalent to that of the hyperhoneycomb one, which supports the common origin of the phase transition on two lattices.

The paper is structured as follows. In Sec. II, we introduce the Kitaev model on a hyperoctagon lattice, and briefly describe the numerical method used in the previous studies to analyze the finite- T properties of the Kitaev model. Then we introduce the improved QMC

method by using the Green-function based KPM (GFb-KPM) and present the benchmark results. In Sec. III, we present numerical results. We identify the finite- T phase transition and estimate the critical temperature from careful analyses of finite-size effects for three different physical quantities. In Sec. IV, we discuss the origin of the phase transition on the hyperoctagon lattice, with a consideration of the anisotropic limit of the model in comparison with that for the hyperhoneycomb case. We also discuss a correlation between the critical temperature and the flux gap, with a brief comment on the ground state. Finally, Sec. V is devoted to the summary.

II. MODEL AND METHOD

We study an extension of the Kitaev model¹⁴ to a 3D hyperoctagon lattice shown in Fig. 1²¹. The Hamiltonian is given by

$$\mathcal{H} = -J_x \sum_{\langle i,j \rangle_x} \sigma_i^x \sigma_j^x - J_y \sum_{\langle i,j \rangle_y} \sigma_i^y \sigma_j^y - J_z \sum_{\langle i,j \rangle_z} \sigma_i^z \sigma_j^z, \quad (1)$$

where σ_i^x , σ_i^y , and σ_i^z are the Pauli matrices describing a spin-1/2 state at site i . The sum $\langle i,j \rangle_\gamma$ is taken over the nearest-neighbor (NN) sites on the three different types of bonds, which are shown by red ($\gamma = x$), green (y), and blue (z) in Fig. 1; J_γ is the exchange constant for each bond. Similar to the original Kitaev model on a honeycomb lattice¹⁴, the hyperoctagon model has a Z_2 conserved quantity called the fluxes for each ten-site plaquette p (see Fig. 1), $W_p = \prod_{\langle i,j \rangle_\gamma \in p} \sigma_i^\gamma \sigma_j^\gamma = \pm 1$, where the product is taken for all the bonds comprising the plaquette. While the ground state of this model is not exactly obtained, it was deduced to be a flux-free state, where all W_p are $+1$ ²¹, similar to the honeycomb¹⁴ and hyperhoneycomb cases¹⁸.

We investigate thermodynamic properties of the model in Eq. (1) by the QMC simulation based on a Majorana fermion representation¹². In this technique, the lattice is regarded as an assembly of one-dimensional chains composed of two types of bonds and the Jordan-Wigner transformation is applied to each chain^{26–28}. By taking such chains along the \mathbf{a}_1 direction composed of the red and green bonds as in Fig. 1, the Kitaev Hamiltonian in Eq. (1) is rewritten by two types of Majorana fermions c and \bar{c} as

$$\mathcal{H} = iJ_x \sum_{(w,b)_x} c_w c_b + iJ_y \sum_{(w,b)_y} c_w c_b + iJ_z \sum_{(w,b)_z} \eta_r c_w c_b, \quad (2)$$

where $\eta_r = i\bar{c}_b c_w$ is a local conserved quantity taking ± 1 (r is the index for the z bond); it satisfies $W_p = \prod_{r \in p} \eta_r$, where the product is taken for all the z bonds included in the ten-site loop. The sum of $(w,b)_\gamma$ is taken for the NN sites on the γ bonds with $w > b$ ($b > w$) if the chain begins with b (w) (see Fig. 1). From the form of Eq. (2), the system is regarded as free Majorana fermions coupled

with the Z_2 variables η_r . Hence, one can compute thermodynamic properties by Monte Carlo (MC) sampling over the configurations $\{\eta_r\}$ with the statistical weight $P(\{\eta_r\}) = \exp[-\beta F(\{\eta_r\})]$, where $F(\{\eta_r\})$ is the free energy of the Majorana fermions $\{c\}$ for a configuration $\{\eta_r\}$, and $\beta = 1/T$ is the inverse temperature (we set the Boltzmann constant $k_B = 1$). As $P(\{\eta_r\})$ is positive definite, the QMC simulation is free from the negative sign problem^{12,17,29,30}.

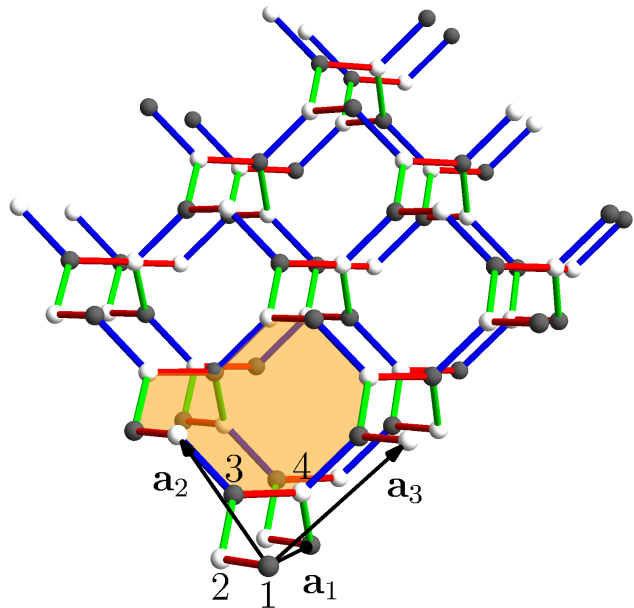


FIG. 1. Schematic picture of the hyperoctagon lattice. The spheres represent the lattice sites on which the spin-1/2 degrees of freedom are defined in Eq. (1). The sites 1-4 represent the four-site unit cell, and \mathbf{a}_μ ($\mu = 1, 2, 3$) represent the lattice translation vectors. The red, green, and blue bonds denote the x , y , and z bonds in Eq. (1), respectively. The hyperoctagon lattice is bipartite, and the black b and white w spheres identify the sublattices; see Eq. (2). The orange shade denotes an example of a ten-site plaquette on which the Z_2 flux W_p is defined.

In the previous studies^{12,17,29,30}, $F(\{\eta_r\})$ was calculated by the exact diagonalization (ED), which leads to the computational cost of $\mathcal{O}(N^4)$ for one MC sweep where N is the number of spins. This has limited the reachable system size N to less than 10^3 in a reasonable computational time. In order to reduce the computational cost and enable systematic analysis of up to larger N , in the present study, we apply the GFb-KPM to estimate $F(\{\eta_r\})$ ³¹. In this method, a change of the Majorana fermion density of states in a MC update is directly computed from a small number of Green functions obtained by the KPM³², which reduces the computational cost to $\mathcal{O}(N^2)$.

Let us describe the method briefly. Suppose if the one-body Majorana Hamiltonian for a given configuration $\{\eta_r\}$, $\mathcal{H}(\{\eta_r\})$, is modified to $\mathcal{H}(\{\eta_r\}) + \Delta$ by a local

flip of η_r , then the energy spectrum is given by the solution of $\mathcal{D}(E) = \det\{\mathbb{I} + G(E)\Delta\} = 0$, where $G(E)$ is the Green function satisfying $G(E)\{\mathcal{H}(\{\eta_r\}) - E\mathbb{I}\} = \mathbb{I}$ (\mathbb{I} is the unit matrix). By extending $\mathcal{D}(E)$ to a complex function by $E \rightarrow E + i\epsilon$, the difference in the free energy by the local flip is given by

$$F(\{\eta'_r\}) - F(\{\eta_r\}) = -\frac{N}{\pi} \int_0^\infty \lim_{\epsilon \rightarrow 0} \text{Im} \ln\{\mathcal{D}(E + i\epsilon)\} \frac{1}{2} \tanh\left(\frac{\beta E}{2}\right) dE. \quad (3)$$

$\mathcal{D}(E + i\epsilon)$ can be calculated in a compact manner by using a few components of Green's functions³². The Green functions are obtained by using the KPM with Chebyshev polynomials. For instance, the onsite component is obtained as

$$G_{j,j}(E + i\epsilon) = i \frac{\mu_0 + 2 \sum_{m=1}^{M-1} \mu_m \exp\{-im \arccos(E/s)\}}{\sqrt{s^2 - E^2}}, \quad (4)$$

where μ_m is the j th diagonal element of the m th Chebyshev moment of $\mathcal{H}(\{\eta_r\})$ rescaled by a factor of s to fit the eigenvalues in the range of $[-1 : 1]$, and M is the cutoff of the expansion³¹. μ_m is calculated efficiently by sparse matrix-vector multiplications³².

In the following calculations, we focus on the isotropic case and set the energy unit as $J_x = J_y = J_z = 1/3$. We consider the clusters from 32 (2^3 unit cells) to 2048 sites (8^3 unit cells) with the open boundary condition in the \mathbf{a}_1 direction and the periodic ones in the remaining two directions. We typically perform ten independent MC runs with 500 MC steps for measurements after 3500 to 5500 steps for thermalization. In addition to MC sweeps by a single flip of η_r , we adopt the replica exchange MC technique³³.

Figure 2 shows the benchmark of the GFb-KPM method. We compare the QMC data of the specific heat per site, C_v , computed by the ED method and the GFb-KPM method for the $4 \times 4^3 = 256$ -site cluster. For the GFb-KPM calculations, we present the data with a different cutoff of the Chebyshev expansion, M , from $M = 64$ to 512. Figure 2(a) shows T dependence of C_v . We find that the GFb-KPM data well converge to the ED ones, even for the smallest $M = 64$, except for the low- T region around the low- T peak of C_v . Figure 2(b) shows the convergence of the GFb-KPM data in terms of M in the low- T region: the symbols indicate the GFb-KPM data for each M , while the horizontal lines the ED ones (the dashed lines indicate the statistical errorbars). We find that the GFb-KPM results quickly converge to the ED ones while increasing M . On the basis of this benchmark as well as the fact that the GFb-KPM converges faster for larger system sizes³², we take $M = 512$ for the 576-site cluster and $M = 256$ for larger clusters in the following GFb-KPM calculations³⁴.

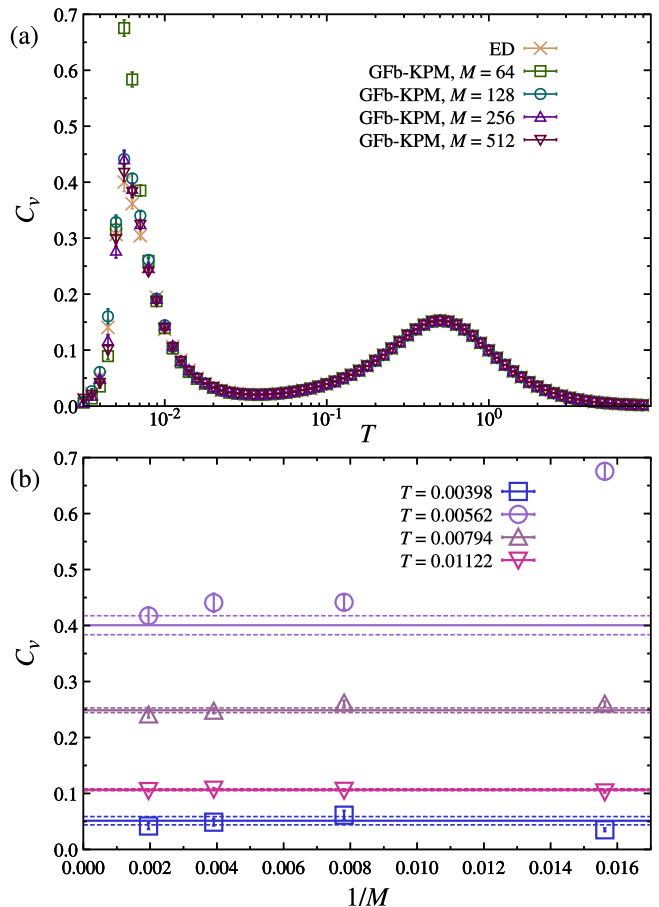


FIG. 2. (a) Comparison of the QMC results for the T dependence of the specific heat per site, C_v , obtained by the update scheme with the ED and GFb-KPM. In the GFb-KPM calculations, the Green functions are obtained by the Chebyshev expansion up to $M = 512$. (b) M dependence of C_v at several temperatures in the low- T region around the low- T peak in (a). The horizontal solid lines represent the ED results with errorbars indicated by the dashed lines. The calculations are done for the isotropic case $J_x = J_y = J_z = 1/3$ in Eq. (1) on the $4 \times 4^3 = 256$ -site cluster.

III. RESULTS

Figure 3(a) shows the QMC results of the specific heat per site, C_v . Similar to the hyperhoneycomb case¹², C_v exhibits two peaks. The higher- T peak is closely related with the development of NN spin correlations $S^{zz} = 2 \sum_{\langle i,j \rangle_z} \langle \sigma_i^z \sigma_j^z \rangle / N$ shown in Fig. 3(c), which corresponds to the lowering of the kinetic energy of the itinerant Majorana fermions^{12,17}. On the other hand, the lower- T peak in C_v is associated with the coherent alignment of the Z_2 variables W_p ^{12,17}; see the thermal average $\bar{W}_p = \langle \sum_p W_p \rangle / N_p$ plotted in Fig. 3(c) (N_p is the number of ten-site plaquettes in the system). Figure 3(b) shows the results of the entropy per site, $S = \ln 2 + \beta \langle \mathcal{H} \rangle / N - \int_0^\beta \langle \mathcal{H} \rangle d\beta / N$. At each peak of C_v ,

a half of $\ln 2$ entropy is released; the higher- T release comes from itinerant Majorana fermions and the lower one comes from Z_2 variables W_p . Similar behavior was reported for the Kitaev models on the honeycomb and hyperhoneycomb lattices^{12,17}. This is the common feature in the Kitaev QSLs called thermal fractionalization of quantum spins¹⁷.

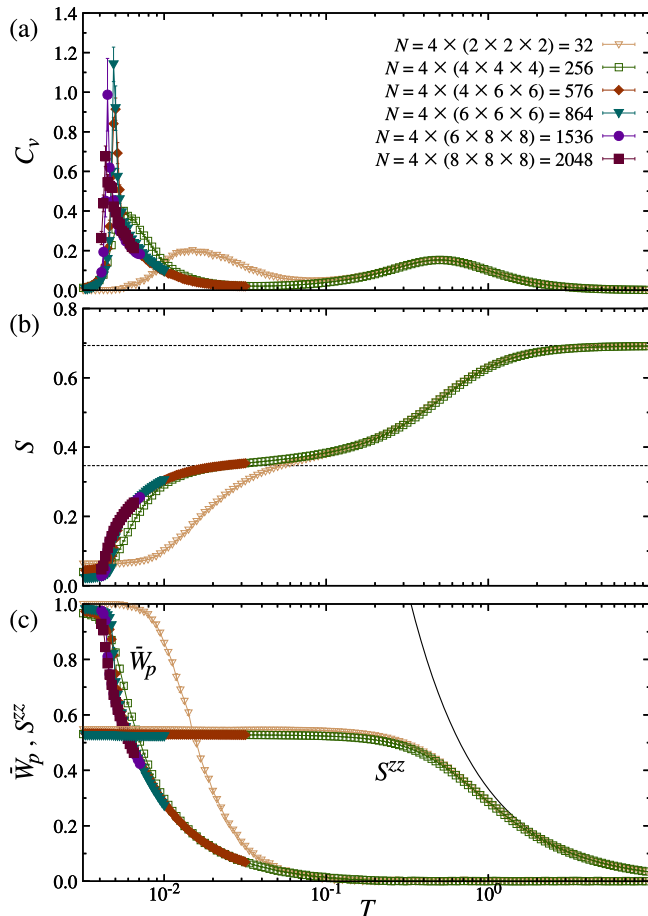


FIG. 3. Temperature dependence of (a) C_v , (b) the entropy per site S , and (c) the average of the Z_2 variables W_p , \bar{W}_p , and the NN spin correlation on the z bonds, S^{zz} . The calculations were performed for the isotropic case in Eq. (1) on several clusters whose sizes are indicated in the figure. The dashed horizontal lines in (b) indicate $(1/2)\ln 2$ and $\ln 2$. The black curve in (c) represents the high- T asymptotic Curie behavior $1/(3T)$.

In Fig. 3(a), while the high- T peak of C_v is almost system-size independent, the low- T peak exhibits significant system-size dependence: the peak becomes sharper and shifts to lower T while increasing the system size. The enlarged view of the low- T part is shown in Fig. 4(a). The system-size dependence is indicative of a phase transition, as in the hyperhoneycomb case¹². We note that the height of the peaks does not show systematic behavior, which is presumably due to the different shapes of clusters. We find similar critical behavior in thermal

fluctuations of W_p , defined by

$$\Delta W_p = \frac{(\sum_{\gamma} J_{\gamma})^2}{N_p T^2} \left[\langle (\sum_p W_p)^2 \rangle - \langle \sum_p W_p \rangle^2 \right]. \quad (5)$$

As shown in Fig. 4(b), ΔW_p shows a similar peak to C_v . We note that this quantity gives a measure of the specific heat in the case of the anisotropic limit of the Kitaev model where the Hamiltonian is described by W_p only; namely, ΔW_p gives a measure of energy fluctuations related to W_p . Thus, the common critical behavior between C_v and ΔW_p indicates that the phase transition is driven by the Z_2 variables W_p .

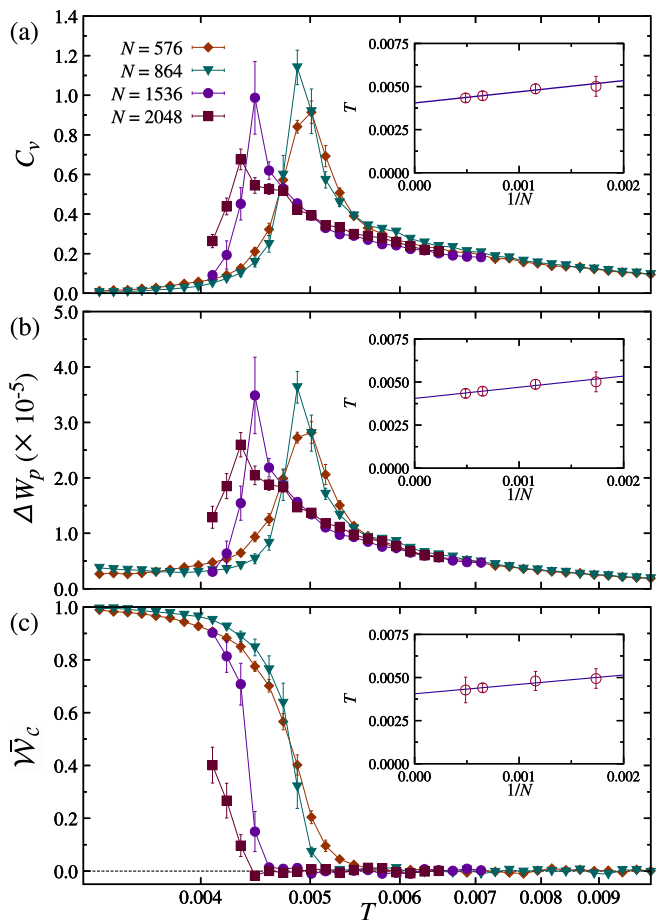


FIG. 4. Enlarged views of the low- T region: (a) C_v , (b) fluctuations of W_p , ΔW_p , and (c) the Wilson loop \bar{W}_c . The insets show the system-size extrapolation of the peak T of (a) C_v and (b) ΔW_p , and (c) the inflection point of T dependence of \bar{W}_c .

In order to characterize the phase transition, following the previous study for the hyperhoneycomb case¹², we also measure the Wilson loop \bar{W}_c on a plane perpendicular to one of the periodic boundaries³⁵. As shown in Fig. 4(c), \bar{W}_c is zero at high T and grows rapidly in well accordance with the peaks of C_v and ΔW_p . This behavior is in contrast to the gradual growth of \bar{W}_p in

Fig. 3(c). The result indicates that the global quantity $\bar{\mathcal{W}}_c$ acts as an order parameter for the unconventional phase transition, as in the hyperhoneycomb case¹².

From the critical behaviors of C_v , ΔW_p , and $\bar{\mathcal{W}}_c$, we estimate the critical temperature T_c . The insets in Fig. 4 present the system-size extrapolation of the peak T of C_v and ΔW_p and the inflection point of T dependence of $\bar{\mathcal{W}}_c$. The extrapolated values to $N \rightarrow \infty$ well coincide with each other: $T_c = 0.00405(10)$ by C_v , $0.00405(10)$ by ΔW_p , and $0.00406(8)$ by $\bar{\mathcal{W}}_c$ (the numbers in the parentheses represent the errors in the last digits). This good agreement indicates the validity of our numerical simulation and the system-size analysis.

IV. DISCUSSION

From the comparison to the previous study for the hyperhoneycomb model¹², we conclude that the phase transition on the hyperoctagon lattice is another realization of the “liquid-gas” phase transition between the low- T QSL and the high- T paramagnet. Similar to the hyperhoneycomb case, we do not observe any indication of discontinuity in the transition³⁶. In the hyperhoneycomb case, the origin of the phase transition is ascribed to a proliferation of closed loops formed by flipped W_p ¹². Such loop excitations are commonly seen in the 3D systems including the hyperoctagon case^{16,21}. Our result suggests that the phase transition takes place universally in the 3D Kitaev models once the low-energy physics is described by closed loops of W_p .

The common phase transition between the hyperoctagon and hyperhoneycomb cases is also inferred by considering the anisotropic limit of the models, $J_z \gg J_x$ and J_y . For both cases, the low-energy effective model is obtained by the similar perturbation theory to that used for the derivation of the toric code from the Kitaev model in Ref. 14. In the perturbation theory, the original Hilbert space is projected onto the low-energy subspace where each dimer made of two spins connected by the strong z bond, say σ_1 and σ_2 , takes only two states out of four; these two states are represented by a pseudospin $|\tau_{ij}^z = \pm 1\rangle = |\sigma_i^z = \sigma_j^z = \pm 1\rangle$. When one defines the pseudospins at the centers of z bonds, the lattice is reduced to the diamond lattice for both hyperoctagon and hyperhoneycomb cases. For the hyperhoneycomb case, the low-energy effective model was obtained in Ref. 18 by considering the eighth-order perturbation. The effective model is described by the projected Z_2 fluxes $B_p = \pm 1$ that are defined for each six-site plaquette in the diamond lattice, and has the form of $\mathcal{H}_{\text{eff}} = -\sum_p J_{\text{eff}}^p B_p$, where J_{eff}^p is either $7J_x^4 J_y^2 / 256 J_z^5$ or $7J_y^4 J_x^2 / 256 J_z^5$ depending on the number of x bond included in the plaquette p . It was numerically demonstrated that the effective model exhibits a finite- T phase transition between the high- T paramagnet and the low- T QSL¹³. Performing the similar procedure, we find that the low-energy effective model for the hyperoctagon case has the same form, except for

the sign of the coupling constant J_{eff}^p . As the opposite sign does not cause any difference in the thermodynamics, the effective model shows the same finite- T phase transition as in the hyperhoneycomb case. Although this correspondence is only in the anisotropic limit, it strongly suggests a common mechanism of the finite- T phase transition between the two models even in the isotropic case.

On the other hand, we note that our estimate of T_c for the hyperoctagon model is lower than that for the hyperhoneycomb case, as shown in Table I¹². As the phase transition is caused by the loop proliferation, T_c is closely related with the loop tension¹⁶. The loop tension is determined by the flux gap Δ , which is defined by the minimum excitation energy for flipping W_p from the ground state. The flux gap is estimated as $\Delta = 0.030(3)$ for the hyperoctagon lattice and $\Delta = 0.043(3)$ for the hyperhoneycomb lattice²⁰. The values of T_c and Δ summarized in Table I indicate a good correlation between T_c and Δ .

Finally, let us briefly comment on the ground state. As shown in Fig. 3(c), our QMC data for \bar{W}_p converge to $+1$ at low T . This suggests that the system is likely to be in the flux-free state with all $W_p = +1$ when $T \rightarrow 0$, as deduced by variational arguments in the previous study²¹.

Lattice	Critical temperature T_c	Flux gap Δ
Hyperoctagon	0.00405(10)	0.030(3)
Hyperhoneycomb	0.00519(9)	0.043(3)

TABLE I. Comparison between the critical temperature T_c obtained by the QMC simulations and the magnitude of the flux gap Δ estimated at $T = 0$ for the hyperhoneycomb and hyperoctagon cases. T_c for the hyperhoneycomb system is taken from Ref. 12, while Δ from Ref. 20.

V. SUMMARY

In summary, we have investigated the “liquid-gas” phase transition from the low- T QSL to the high- T paramagnet on the extension of the Kitaev model to the 3D hyperoctagon lattice. Using an improved QMC method by the Green function technique with the KPM, we successfully dealt with much larger-size systems compared to the previous studies. From the systematic analysis of clusters up to 2048 sites, we found a finite- T phase transition similar to the previous hyperhoneycomb case. The result was also supported by considering the anisotropic limit of the model on two lattices. We also showed that the critical temperature on the hyperoctagon lattice is lower than in the hyperhoneycomb case, reflecting the smaller flux gap in the former case. It will be interesting to extend the present study to other 3D Kitaev models for an exploration of further exotic phase transitions.

ACKNOWLEDGMENTS

The authors thank J. Nasu, R. Ozawa, and J. Yoshitake for fruitful discussions. This research was supported

by JSPS Grants-in-Aid for Scientific Research Grants No. JP15K13533, No. JP16H02206, and No. 26800199. Parts of the numerical calculations were performed in the supercomputing systems in ISSP, the University of Tokyo.

-
- ¹ P. W. Anderson, “Resonating valence bonds: A new kind of insulator?,” *Mater. Res. Bull.* **8**, 153 (1973).
- ² P. Fazekas and P. W. Anderson, “On the ground state properties of the anisotropic triangular antiferromagnet,” *Phil. Mag.* **30**, 423 (1974).
- ³ L. Balents, “Spin liquids in frustrated magnets,” *Nature (London)* **464**, 199 (2010).
- ⁴ K. Kanoda and R. Kato, “Mott Physics in Organic Conductors with Triangular Lattices,” *Annu. Rev. Condens. Matter Phys.* **2**, 167 (2011).
- ⁵ M. J. P. Gingras and P. A. McClarty, “Quantum spin ice: a search for gapless quantum spin liquids in pyrochlore magnets,” *Rep. Prog. Phys.* **77**, 056501 (2014).
- ⁶ Y. Okamoto, M. Nohara, H. Aruga-Katori, and H. Takagi, “Spin-Liquid State in the $S = 1/2$ Hyperkagome Antiferromagnet $\text{Na}_4\text{Ir}_3\text{O}_8$,” *Phys. Rev. Lett.* **99**, 137207 (2007).
- ⁷ R. Coldea, D. A. Tennant, and Z. Tylczynski, “Extended scattering continua characteristic of spin fractionalization in the two-dimensional frustrated quantum magnet Cs_2CuCl_4 observed by neutron scattering,” *Phys. Rev. B* **68**, 134424 (2003).
- ⁸ Z. Hiroi, M. Hanawa, N. Kobayashi, M. Nohara, H. Takagi, Y. Kato, and M. Takigawa, “Spin-1/2 Kagome-Like Lattice in Volborthite $\text{Cu}_3\text{V}_2\text{O}_7(\text{OH})_2 \cdot 2\text{H}_2\text{O}$,” *J. Phys. Soc. Jpn.* **70**, 3377 (2001).
- ⁹ M. P. Shores, E. A. Nytko, B. M. Bartlett, and D. G. Nocera, “A Structurally Perfect $S = 1/2$ Kagome Antiferromagnet,” *J. Am. Chem. Soc.* **127**, 13462 (2005).
- ¹⁰ Y. Okamoto, H. Yoshida, and Z. Hiroi, “Vesignieite $\text{BaCu}_3\text{V}_2\text{O}_8(\text{OH})_2$ as a Candidate Spin-1/2 Kagome Antiferromagnet,” *J. Phys. Soc. Jpn.* **78**, 033701 (2009).
- ¹¹ T.-H. Han, J. Singleton, and J. A. Schlueter, “Barlowite: A Spin-1/2 Antiferromagnet with a Geometrically Perfect Kagome Motif,” *Phys. Rev. Lett.* **113**, 227203 (2014).
- ¹² J. Nasu, M. Udagawa, and Y. Motome, “Vaporization of Kitaev Spin Liquids,” *Phys. Rev. Lett.* **113**, 197205 (2014).
- ¹³ J. Nasu, T. Kaji, K. Matsuura, M. Udagawa, and Y. Motome, “Finite-temperature phase transition to a quantum spin liquid in a three-dimensional Kitaev model on a hyperhoneycomb lattice,” *Phys. Rev. B* **89**, 115125 (2014).
- ¹⁴ A. Kitaev, “Anyons in an exactly solved model and beyond,” *Ann. Phys. (N.Y.)* **321**, 2 (2006).
- ¹⁵ G. Jackeli and G. Khaliullin, “Mott Insulators in the Strong Spin-Orbit Coupling Limit: From Heisenberg to a Quantum Compass and Kitaev Models,” *Phys. Rev. Lett.* **102**, 017205 (2009).
- ¹⁶ I. Kimchi, J. G. Analytis, and A. Vishwanath, “Three-dimensional quantum spin liquids in models of harmonic-honeycomb iridates and phase diagram in an infinite- D approximation,” *Phys. Rev. B* **90**, 205126 (2014).
- ¹⁷ J. Nasu, M. Udagawa, and Y. Motome, “Thermal fractionalization of quantum spins in a Kitaev model: Temperature-linear specific heat and coherent transport of Majorana fermions,” *Phys. Rev. B* **92**, 115122 (2015).
- ¹⁸ S. Mandal and N. Surendran, “Exactly solvable Kitaev model in three dimensions,” *Phys. Rev. B* **79**, 024426 (2009).
- ¹⁹ S. Yang, D. L. Zhou, and C. P. Sun, “Mosaic spin models with topological order,” *Phys. Rev. B* **76**, 180404(R) (2007).
- ²⁰ K. O’Brien, M. Hermanns, and S. Trebst, “Classification of gapless Z_2 spin liquids in three-dimensional Kitaev models,” *Phys. Rev. B* **93**, 085101 (2016).
- ²¹ M. Hermanns and S. Trebst, “Quantum spin liquid with a Majorana Fermi surface on the three-dimensional hyperoctagon lattice,” *Phys. Rev. B* **89**, 235102 (2014).
- ²² H. Yao and S. A. Kivelson, “Exact Chiral Spin Liquid with Non-Abelian Anyons,” *Phys. Rev. Lett.* **99**, 247203 (2007).
- ²³ G. Baskaran, S. Mandal, and R. Shankar, “Exact Results for Spin Dynamics and Fractionalization in the Kitaev Model,” *Phys. Rev. Lett.* **98**, 247201 (2007).
- ²⁴ E. H. Lieb, “Flux Phase of the Half-Filled Band,” *Phys. Rev. Lett.* **73**, 2158 (1994).
- ²⁵ A. F. Wells, *Three Dimensional Nets and Polyhedra*, 1st ed. (John Wiley and Sons Inc., New York, 1977).
- ²⁶ H.-D. Chen and J. Hu, “Exact mapping between classical and topological orders in two-dimensional spin systems,” *Phys. Rev. B* **76**, 193101 (2007).
- ²⁷ X.-Y. Feng, G.-M. Zhang, and T. Xiang, “Topological Characterization of Quantum Phase Transitions in a Spin-1/2 Model,” *Phys. Rev. Lett.* **98**, 087204 (2007).
- ²⁸ H.-D. Chen and Z. Nussinov, “Exact results of the Kitaev model on a hexagonal lattice: spin states, string and brane correlators, and anyonic excitations,” *J. Phys. A* **41**, 075001 (2008).
- ²⁹ J. Nasu and Y. Motome, “Thermodynamics of Chiral Spin Liquids with Abelian and Non-Abelian Anyons,” *Phys. Rev. Lett.* **115**, 087203 (2015).
- ³⁰ J. Nasu, J. Knolle, D. L. Kovrizhin, Y. Motome, and R. Moessner, “Fermionic response from fractionalization in an insulating two-dimensional magnet,” *Nature Physics* **12**, 912 (2016).
- ³¹ A. Weiße, “Green-Function-Based Monte Carlo Method for Classical Fields Coupled to Fermions,” *Phys. Rev. Lett.* **102**, 150604 (2009).
- ³² A. Weiße, G. Wellein, A. Alvermann, and H. Fehske, “The kernel polynomial method,” *Rev. Mod. Phys.* **78**, 275 (2006).
- ³³ K. Hukushima and K. Nemoto, “Exchange Monte Carlo Method and Application to Spin Glass Simulations,” *J. Phys. Soc. Jpn.* **65**, 1604 (1996).
- ³⁴ We compute the two smallest clusters with $N = 32$ and 256 by QMC with ED.
- ³⁵ We define \mathcal{W}_c on a half of the largest loop on the plane which is halved in the periodic boundary condition.

³⁶ We carefully examine the histogram of the internal energy, but do not find any clear signature of bifurcation.